https://doi.org/10.15407/ujpe69.4.232

M. AYGUN,[1] Z. AYGUN,[2] N. KARAALI[1]

[1] Department of Physics, Bitlis Eren University
(Bitlis, Türkiye)

[2] Vocational School of Technical Sciences, Bitlis Eren University
(13000 Bitlis, Türkiye; e-mail: murata.25@gmail.com)

AN EXTENDED ANALYSIS OF ^{14}N(^{17}F, ^{18}Ne)^{13}C, AND ^{14}N(^{7}Be, ^{8}B)^{13}C PROTON-TRANSFER REACTIONS DEPENDING ON THE TEMPERATURE, DENSITY DISTRIBUTION, NUCLEAR POTENTIAL, AND NUCLEON-NUCLEON INTERACTIONS

The angular distributions of $^{14}N(^{17}F, ^{18}Ne)^{13}C$ at 170 MeV and $^{14}N(^{7}Be, ^{8}B)^{13}C$ at 84 MeV proton-transfer reactions depending on the density distributions, temperature, nuclear potentials, and nucleon-nucleon interactions are studied. The calculations are performed by using the code FRESCO based on the distorted wave Born approximation (DWBA) method. The theoretical results of all the approaches are compared with both each other and experimental data, and the similarities and differences of the results are discussed. Additionally, new potential parameter sets for the description of the experimental data of each reaction are developed. Finally, alternative density, nuclear potential, and nucleon-nucleon interactions are proposed for the analysis of the angular distributions of the $^{14}N(^{17}F, ^{18}Ne)^{13}C$ and $^{14}N(^{7}Be, ^{8}B)^{13}C$ proton-transfer reactions.

K e y w o r d s: transfer reaction, density distribution, nuclear potential, nucleon-nucleon interaction.

1. Introduction

Nuclear astrophysics seeks answers to fundamental questions in nature. For example, what generates the elements that form both body and world? How did the Sun, stars, and the galaxy come into being? How are they developing? Nuclear reactions are liable for the formation of the elements in the cosmos [1,2]. In this way, nuclear experimental measurements can contribute to explaining the complex theoretical models of the astrophysical systems [3]. Therefore, theoretical analysis of nuclear reactions is of a great significance, as they give us the information about both nuclear structure and reaction dynamics.

Nuclear astrophysics studies need nuclear inputs such as charged-particle cross-sections which are very significant and are also difficult to be measured due to the low energies and cross-sections [4]. In this context, transfer reactions occupy a special place for nuclear physics and nuclear astrophysics. They can provide a structural information to input in astrophysical simulations. Additionally, it can be evaluated as an indirect method in order to obtain capture reaction rates for stellar temperatures [5–8].

Proton-transfer reactions play a specially substantial role in the definition of nuclei. The ^{14}N(^{17}F, ^{18}Ne)^{13}C and ^{14}N(^{7}Be, ^{8}B)^{13}C reactions are some of the important proton-transfer reactions. The ^{14}N(^{17}F, ^{18}Ne)^{13}C reaction can be evaluated to extract the asymptotic normalization coefficients (ANC) of specific states of ^{18}Ne which can give a undeniable part of the rate for the ^{17}F(p, γ)^{18}Ne reaction [9, 10]. The proton-capture reaction by the ^{17}F nucleus can seem in the rp-process in a novae envi-

Citation: Aygun M., Aygun Z., Karaali N. An extended analysis of ^{14}N(^{17}F, ^{18}Ne)^{13}C and ^{14}N(^{7}Be, ^{8}B)^{13}C proton transfer reactions depending on the temperature, density distribution, nuclear potential and nucleon-nucleon interactions. *Ukr. J. Phys.* **69**, No. 4, 232 (2024). https://doi.org/10.15407/ujpe69.4.232.

Цитування: Айгун М., Айгун З., Караалі Н. Повний аналіз реакцій ^{14}N(^{17}F, ^{18}Ne)^{13}C та ^{14}N(^{7}Be, ^{8}B)^{13}C з передачею протона, які залежать від температури, розподілу густини, ядерного потенціалу і взаємодії між нуклонами. *Укр. фіз. журн.* **69**, №4, 232 (2024).

ronments, and is an significant phase in the hot CNO cycle of both novae and x-ray bursts [11]. Novae are the most joint stellar explosions in the Galaxy, and generate some light isotopes which are hard to be fabricated in other environments [12]. Additionally, the ratio of the proton capture and decay rates of ^{17}F are also crucial to understanding galactic ^{17}O, ^{18}O and ^{15}N [9]. It has a determinative influence on the abundances of ^{17}F, ^{18}F and ^{18}Ne, and defines the ^{17}O/^{18}O ratio in explosive hydrogen burning [13].

The ^{14}N(^{7}Be, ^{8}B)^{13}C proton-transfer reaction is significant to obtain the enough information about ^{8}B which has a proton halo structure with a binding energy of only 137 keV of its last proton. The ^{8}B nucleus, which is obtained by means of the ^{7}Be(p,γ)^{8}B reaction in the Sun, is the source of high energy neutrinos [14]. Azhari *et al.* [15] measured the experimental data of the ^{14}N(^{7}Be, ^{8}B)^{13}C transfer reaction. They obtained the ANC for ^{7}Be + p $\Rightarrow$ $\Rightarrow$ ^{8}B which is used to understand the astrophysical S factor for the ^{7}Be(p, γ)^{8}B capture reaction at solar energies $S_{17}(0)$. Moro *et al.* [16, 17] studied the breakup and core coupling in the ^{14}N(^{7}Be, ^{8}B)^{13}C reaction. They reported on an insignificant effect of the breakup of the ^{8}B nucleus for ^{14}N(^{7}Be, ^{8}B)^{13}C. They also showed that the spin, excitation, and deformation of the core have a small effect for the transfer reaction. However, it was seen that some important aspects such as a density distribution (DD), the temperature, nuclear potential, and nucleon interactions were not examined simultaneously and comprehe]nsively, when the studies on these two important reactions were searched in the literature. We believe that eliminating the absence in the literature will make valuable contributions to future studies with these reactions.

In the present study, we analyze the cross-sections of the ^{14}N(^{17}F, ^{18}Ne)^{13}C at 170 MeV and ^{14}N(^{7}Be, ^{8}B)^{13}C at 84 MeV proton-transfer reactions for temperature-dependent (TD) and temperature-independent (T-IND) DDs, different nuclear potentials, and different nucleon-nucleon (NN) interactions. The theoretical calculations are performed by using the code FRESCO [18] based on the distorted wave Born approximation (DWBA) method. The theoretical results and the experimental data are compared with each other, and alternative density, nuclear potential, and NN interactions are proposed. Additionally, new potential parameters for the

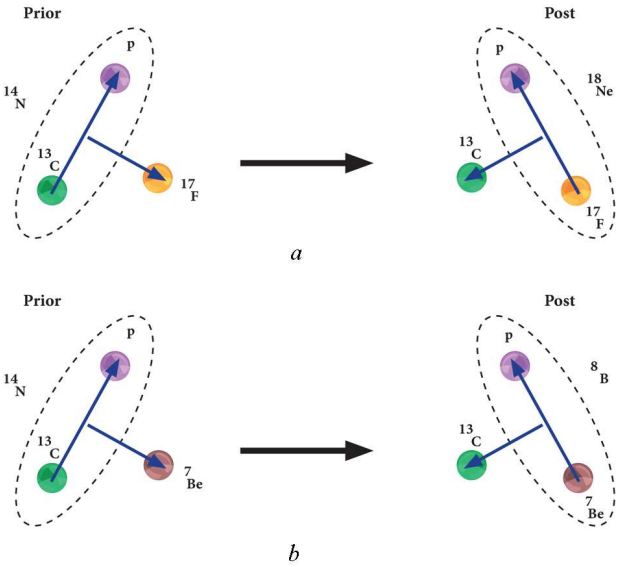

Fig. 1. The scheme of ^{14}N(^{17}F,^{18}Ne)^{13}C (*a*), ^{14}N(^{7}Be, ^{8}B)^{13}C (*b*)

description of the experimental data on each proton-transfer reaction are developed.

Section 2 displays the theory of transfer reaction channels. Sections 3 and 4 present the TD and T-IND DDs, respectively. Sections 5 and 6 give the theory of different nuclear potentials and NN interactions, respectively. Section 7 shows the results and discussion. Section 8 exhibits the summary and conclusions.

2. Theory of Transfer Reaction Channels

In the analysis of the ^{14}N(^{17}F, ^{18}Ne)^{13}C and ^{14}N(^{7}Be, ^{8}B)^{13}C transfer reactions, the various interactions such as the entrance channel, exit channel, core-core and binding potentials are handled. In this way, the ^{14}N(^{17}F, ^{18}Ne)^{13}C reaction is considered; entrance channel (^{17}F + ^{14}N), exit channel (^{18}Ne + + ^{13}C), core-core (^{17}F + ^{13}C), and binding potentials (p + ^{13}C and p + ^{17}F). The ^{14}N target is assumed as a composite system ^{14}N = p + ^{13}C (see Fig. 1, *a*) in the entrance channel. Then one p is transferred to the ^{17}F projectile, and the composite state ^{18}Ne = = ^{17}F + p occurs in the exit channel.

The ^{14}N(^{7}Be, ^{8}B)^{13}C reaction is accepted as; entrance channel (^{7}Be + ^{14}N), exit channel (^{8}B + ^{13}C), core-core (^{7}Be + ^{13}C), binding potentials (p + ^{13}C and p + ^{7}Be). ^{14}N is assumed as the composite system ^{14}N = p + ^{13}C (see Fig. 1, *b*) in the entrance

channel. Then one p is transferred to the ^{7}Be projectile, and the composite state ^{8}B = ^{7}Be + p occurs in the exit channel. The calculation procedures for all the channels of both ^{14}N(^{17}F, ^{18}Ne)^{13}C and ^{14}N(^{7}Be, ^{8}B)^{13}C are described below.

2.1. Entrance Channel

We study the effect of the entrance channel on the transfer cross-section by using different approaches, whose entrance channel potentials are evaluated as important inputs in the analysis of the transfer reactions.

The entrance channel potential contains the real and imaginary potentials. To form the real potential, both optical model (OM) and double folding model (DFM) are used via the codes FRESCO and DFPOT [19] which are used widely in the analysis of various nuclear reactions [20–26]. The real part is calculated for TD and T-IND densities, different nuclear potentials and NN interactions, as summarized in the following sections.

The imaginary potential for the ^{17}F + ^{14}N and ^{7}Be + ^{14}N channels is considered as the Woods–Saxon (WS) volume form

$$W(r) = -\frac{W_0}{\left[1+\exp\left(\frac{r-R_w}{a_w}\right)\right]}, \quad (1)$$

where W_0, R_w and a_w are the depth, the radius and diffuseness parameter, respectively. Additionally, the spin-orbit potential for the real part of the ^{17}F + ^{14}N channel is assumed and written as

$$V_{\rm so}(r) = -\left(\frac{\hbar}{m_\pi c}\right)^2 (\mathbf{L}\,\mathbf{S})\,\frac{V_{\rm so}}{a_{\rm so} r}\,\frac{\exp\left(\frac{r-R_{\rm so}}{a_{\rm so}}\right)}{\left[1+\exp\left(\frac{r-R_{\rm so}}{a_{\rm so}}\right)\right]^2}, \quad (2)$$

where $V_{\rm so}$, $R_{\rm so}$ and $a_{\rm so}$ is the depth, radius, and diffuseness parameters of the spin-orbit potential, respectively.

2.2. Exit Channel

The nuclear potential of the ^{18}Ne + ^{13}C and ^{8}B + + ^{13}C exit channels consists of two parts: real and imaginary ones. In this context, the real part of the optical potential (OP) is taken in the following form:

$$V(r) = \frac{V_0}{\left[1+\exp\left(\frac{r-R_v}{a_v}\right)\right]}. \quad (3)$$

The imaginary potential has the same form with Eq. (1).

2.3. Core-Core

The core-core potentials for ^{17}F + ^{13}C and ^{7}Be + + ^{13}C, which mean the interaction between cores of nuclei, contains the real and imaginary potentials which are in the same form with the potentials of the exit channel.

2.4. Binding potentials

Finally, the binding potentials for the ^{14}N(^{17}F, ^{18}Ne)^{13}C and ^{14}N(^{7}Be, ^{8}B)^{13}C transfer reactions, can be evaluated as binding potential of both entrance and exit channels. Only the real potential is assumed and taken as the same form with Eq. (3). The depths are determined from the binding energies.

3. ^{17}F and ^{7}Be Density Distributions

In our study, we examine the effect of DDs on the cross-sections of the ^{14}N(^{17}F, ^{18}Ne)^{13}C and ^{14}N(^{7}Be, ^{8}B)^{13}C transfer reactions. We would like to point out that the DDs of the ^{17}F and ^{7}Be nuclei studied here are T-IND DDs. In this manner, we have searched for the appropriate DD for the ^{17}F and ^{7}Be nuclei in the literature. As a result, we have found six different densities (Gupta 1 (G1), Gupta 2 (G2), São Paulo (SP), two parameter Fermi (2pF), Ngo-Ngo (Ngo) and Schechter (S)) for the ^{17}F projectile and five different densities (Variational Monte Carlo (VMC), Gupta 1 (G1), Gupta 2 (G2), Ngo-Ngo (Ngo), and Schechter (S)) for the ^{7}Be projectile. All the densities of both ^{17}F and ^{7}Be are summarized below. On the other hand, the DD of the ^{14}N target nucleus is evaluated as

$$\rho(r) = \frac{\rho_0}{1+\exp\left(\frac{r-c}{z}\right)}, \quad (4)$$

where ρ_0, c and z parameters are 0.214639 fm^{-3}, 2.20079 fm, and 0.475549 fm, respectively [27].

3.1. Gupta 1 (G1) and Gupta 2 (G2)

G1 [27, 28] and G2 [29] are formulated by

$$\rho(r) = \frac{\frac{3A_i}{4\pi R_{0i}^3}\left(1+\frac{\pi^2 a_i^2}{R_{0i}^2}\right)^{-1}}{1+\exp\left(\frac{r-R_{0i}}{a_i}\right)}, \quad (5)$$

where

$$R_{0i} \quad \text{and} \quad a_i = a + bA_i - cA_i^2 + dA_i^3 - eA_i^4. \tag{6}$$

The R_{0i} and a_i parameters are taken from Ref. [24].

3.2. São Paulo (SP) and Two parameter Fermi (2pF)

The SP density is described as [30]

$$\rho_i(r) = \frac{\rho_{0i}}{1 + \exp\left(\frac{r-R_i}{a_i}\right)}, \quad (i = n, p), \tag{7}$$

where

$$R_n = 1.49N^{1/3} - 0.79, \quad R_p = 1.81Z^{1/3} - 1.12, \tag{8}$$
$$a_n = 0.47 + 0.00046N, \quad a_p = 0.47 - 0.00083Z. \tag{9}$$

The $R_{n(p)}$ and $a_{n(p)}$ parameters of the 2pF density are given by [31]

$$R_n = 0.953N^{1/3} + 0.015Z + 0.774,$$
$$a_n = 0.446 + 0.0072\left(\frac{N}{Z}\right), \tag{10}$$

$$R_p = 1.322Z^{1/3} + 0.007N + 0.022,$$
$$a_p = 0.449 + 0.0071\left(\frac{Z}{N}\right). \tag{11}$$

3.3. Ngo-Ngo (Ngo)

Ngo can be formulated as [32, 33]

$$\rho_i(r) = \frac{\rho_{0i}}{1 + \exp\left(\frac{r-C}{0.55}\right)}, \quad (i = n, p) \tag{12}$$

where

$$\rho_{0n(0p)} = \frac{3}{4\pi}\frac{N(Z)}{A}\frac{1}{r_{0n(0p)}^3}, \quad C = R\left(1 - \frac{1}{R^2}\right),$$
$$R = \frac{NR_n + ZR_p}{A}, \tag{13}$$

with

$$R_n = (1.1375 + 1.875 \times 10^{-4}A)A^{1/3},$$
$$R_p = 1.128A^{1/3}. \tag{14}$$

3.4. Schechter (S)

The parameters of the S density like the 2pF density are applied as [34]

$$\rho_0 = 0.151177 \text{ fm}^{-3}, \quad R_0 = 2.67413 \text{ fm},$$
$$a = 0.54 \text{ fm for } ^{17}\text{F}, \tag{15}$$

$$\rho_0 = 0.122762 \text{ fm}^{-3}, \quad R_0 = 1.98945 \text{ fm},$$
$$a = 0.54 \text{ fm for } ^{7}\text{Be}. \tag{16}$$

3.5. The Variational Monte Carlo (VMC)

The VMC density reported by Steven *et al.* [35] is taken from Ref. [36].

4. Temperature Dependent (TD) Density

We examine temperature-dependent case of the entrance channel of the $^{14}\text{N}(^{17}\text{F}, ^{18}\text{Ne})^{13}\text{C}$ and $^{14}\text{N}(^{7}\text{Be}, ^{8}\text{B})^{13}\text{C}$ reactions. We apply temperature-dependent 2pF density [37]

$$\rho_i(r) = \frac{\rho_{0i}(T)}{\left[1 + \exp\left(\frac{r-R_{0i}(T)}{a_i(T)}\right)\right]},$$
$$\rho_{0i}(T) = \frac{3A_i}{4\pi R_{0i}^3(T)}\left[1 + \frac{\pi^2 a_i^2(T)}{R_{0i}^2(T)}\right]^{-1}, \tag{17}$$

where $R_{0i}(T = 0)$ and $a_i(T = 0)$ parameters are the same as in Eq. (6) based on the parameters of the G1 density.

To form the real potential at various temperatures, we use TD cases of $R_{0i}(T)$ and $a_i(T)$ equations given by [38]

$$R_{0i}(T) = R_{0i}(T = 0)[1 + 0.0005T^2],$$
$$a_i(T) = a_i(T = 0)[1 + 0.01T^2]. \tag{18}$$

5. Proximity Potentials

Here, we research the effect on the cross-sections of the nuclear potentials obtained by using nine various proximity potentials for the entrance channels of the $^{14}\text{N}(^{17}\text{F}, ^{18}\text{Ne})^{13}\text{C}$ and $^{14}\text{N}(^{7}\text{Be}, ^{8}\text{B})^{13}\text{C}$ proton-transfer reactions. All the potentials are summarized below.

5.1. Proximity 1977 (Prox 77) and Proximity 1988 (Prox 88)

Prox 77 potential [39, 40] is written as

$$V_N^{\text{Prox 77}}(r) = 4\pi\gamma b\frac{C_1C_2}{C_1+C_2}\Phi\left(\zeta = \frac{r - C_1 - C_2}{b}\right) \text{MeV}, \tag{19}$$

where

$$C_i = R_i\left[1 - \left(\frac{b}{R_i}\right)^2 + ...\right],$$
$$R_i = 1.28A_i^{1/3} - 0.76 + 0.8A_i^{-1/3} \text{ fm } (i = 1, 2). \tag{20}$$

The surface energy coefficient, γ, is assumed as

$$\gamma = \gamma_0 \left[1 - k_s \left(\frac{N-Z}{N+Z}\right)^2\right], \tag{21}$$

where $N(Z)$, respectively, is total number of neutrons(protons), $\gamma_0 = 0.9517$ MeV/fm^2, $k_s = 1.7826$ for Prox 77 [41], and $\gamma_0 = 1.2496$ MeV/fm^2, $k_s = 2.3$ for Prox 88 [42]. The universal function $\Phi(\zeta)$ is in the following form:

$$\Phi(\zeta) = \\ = \begin{cases} -\frac{1}{2}(\zeta - 2.54)^2 - 0.0852(\zeta - 2.54)^3, \ \zeta \le 1.2511, \\ -3.437 \ \exp\left(-\frac{\zeta}{0.75}\right), \ \zeta \ge 1.2511. \end{cases} \tag{22}$$

5.2. Broglia and Winther 1991 (BW 91) and Akyüz–Winther (AW 95)

BW 91 [42] is taken as [43]

$$V_N^{\mathrm{BW\,91}}(r) = -\frac{V_0}{\left[1 + \exp\ \left(\frac{r-R_0}{a}\right)\right]} \ \mathrm{MeV}, \\ V_0 = 16\pi \frac{R_1 R_2}{R_1 + R_2} \gamma a, \quad a = 0.63 \, \mathrm{fm}, \tag{23}$$

where

$$R_0 = R_1 + R_2 + 0.29, \\ R_i = 1.233 A_i^{1/3} - 0.98 A_i^{-1/3} \quad (i = 1, 2), \tag{24}$$

and γ is

$$\gamma = 0.95 \left[1 - 1.8 \left(\frac{N_p - Z_p}{A_p}\right)\left(\frac{N_t - Z_t}{A_t}\right)\right]. \tag{25}$$

The difference between AW 95 and BW 91 potentials [43, 44] is in the following form:

$$a = \left[\frac{1}{1.17(1 + 0.53(A_1^{-1/3} + A_2^{-1/3}))}\right] \mathrm{fm}, \\ R_0 = R_1 + R_2, \ R_i = 1.2 A_i^{1/3} - 0.09. \tag{26}$$

5.3. Bass 1973 (Bass 73), Bass 1977 (Bass 77) and Bass 1980 (Bass 80)

Bass 73 potential [45, 46] can be written as [40]

$$V_N^{\mathrm{Bass\,73}}(r) = -\frac{22.95(A_1^{1/3} A_2^{1/3})}{1.07(A_1^{1/3} + A_2^{1/3})} \times \\ \times \exp\left(-\frac{r - 1.07(A_1^{1/3} + A_2^{1/3})}{1.35}\right) \ \mathrm{MeV}. \tag{27}$$

Bass 77 potential [47] is assumed as [43]

$$V_N^{\mathrm{Bass\,77}}(s) = -\frac{R_1 R_2}{R_1 + R_2} \phi(s = r - R_1 - R_2) \ \mathrm{MeV}, \tag{28}$$

where

$$R_i = 1.16 A_i^{1/3} - 1.39 A_i^{-1/3} \quad (i = 1, 2), \\ \phi(s) = \left[0.030 \exp\left(\frac{s}{3.30}\right) + 0.0061 \exp\left(\frac{s}{0.65}\right)\right]^{-1}. \tag{29}$$

The differences between Bass 80 and Bass 77 [42, 43] are the function $\phi(s = r - R_1 - R_2)$

$$\phi(s) = \left[0.033 \exp\left(\frac{s}{3.5}\right) + 0.007 \ \exp\left(\frac{s}{0.65}\right)\right]^{-1}, \tag{30}$$

and

$$R_i = R_s \left(1 - \frac{0.98}{R_s^2}\right), \\ R_s = 1.28 A_i^{1/3} - 0.76 + 0.8 A_i^{-1/3} \, \mathrm{fm}. \tag{31}$$

5.4. Christensen and Winther 1976 (CW 76)

CW 76 [48] is in the following form: [40]

$$V_N^{\mathrm{CW\,76}}(r) = -50 \frac{R_1 R_2}{R_1 + R_2} \phi(s = r - R_1 - R_2) \ \mathrm{MeV}, \tag{32}$$

where

$$R_i = 1.233 A_i^{1/3} - 0.978 A_i^{-1/3} \ \mathrm{fm} \ (i = 1, 2), \\ \phi(s) = \exp\left(-\frac{r - R_1 - R_2}{0.63}\right). \tag{33}$$

5.5. Ngô 1980 (Ngo 80)

Ngo 80 is parameterized by [32]

$$V_N^{\mathrm{Ngo\,88}}(r) = \frac{\xi_1 \xi_2}{\xi_1 + \xi_2} \phi(r - \xi_1 - \xi_2) \ \mathrm{MeV}, \\ \xi_i = R_i \left[1 - \left(\frac{b}{R_i}\right)^2 + ...\right], \tag{34}$$

and

$$R_i = \frac{(1.1375 + 1.875 \times 10^{-4} A_i) N A_i^{1/3} + 1.128 Z A_i^{1/3}}{A_i} \tag{35}$$

$\phi(\varsigma = r - \xi_1 - \xi_2)$ can be formulated as

$$\Phi(\varsigma) = \begin{cases} -33 + 5.4(\varsigma + 1.6)^2, & \text{for } \varsigma < -1.6, \\ -33 \exp\left[-\frac{1}{5}(\varsigma + 1.6)^2\right] & \text{for } \varsigma \ge -1.6. \end{cases} \tag{36}$$

6. Nucleon-Nucleon (NN) Interactions

We also investigate the impact of eleven different effective NN interactions on the cross-sections which consist of the HS [49], Z [49], W [49], L1 [49], L2 [49], L3 [49], TS [50], NL1 [49], NL2 [49], NL3 [51] and NL3* [52]. As a result of this, we can discuss the similarities and differences of various NN interactions in the analysis of proton-transfer reactions.

The effective NN interaction is taken as the sum of scalar and vector parts of the single meson fields given by [53–55]

$$\nu_{NN}(r) = \frac{g_w^2}{4\pi}\frac{e^{-m_w r}}{r} + \frac{g_\rho^2}{4\pi}\frac{e^{-m_\rho r}}{r} - \frac{g_\sigma^2}{4\pi}\frac{e^{-m_\sigma r}}{r} + \\ + \frac{g_2^2}{4\pi} r e^{-2m_\sigma r} + \frac{g_3^2}{4\pi} r \frac{e^{-3m_\sigma r}}{r}, \tag{37}$$

where g_w, g_ρ, and g_σ are the coupling constants, and m_w, m_ρ and m_σ are the masses for w, ρ, and σ mesons, respectively. With the addition of the single nucleon exchange effect, the equation (37) is

$$\nu_{NN}(r) = \frac{g_w^2}{4\pi}\frac{e^{-m_w r}}{r} + \frac{g_\rho^2}{4\pi}\frac{e^{-m_\rho r}}{r} - \frac{g_\sigma^2}{4\pi}\frac{e^{-m_\sigma r}}{r} + \\ + \frac{g_2^2}{4\pi} r e^{-2m_\sigma r} + \frac{g_3^2}{4\pi} r \frac{e^{-3m_\sigma r}}{r} + \\ + 276\left[1 - 0.005\frac{E_{\rm Lab}}{A_p}\right]\delta(r), \tag{38}$$

where $E_{\rm Lab}$ and A_p are the incident energy and mass number of the projectile, respectively.

7. Results and Discussion

The calculations are carried out using the code FRESCO based on the DWBA method. The calculations of the $^{14}N(^{17}F, ^{18}Ne)^{13}C$ and $^{14}N(^{7}Be, ^{8}B)^{13}C$ reactions are composed of four different stages. We have first applied as starting values of the OP parameters reported in the literature [9, 17]. Then we have carried out the parameter search to success the best-fit with the experimental data. In order to reduce ambiguity in the fitting procedure, the geometrical parameters (radius and diffuseness) are usually fixed to average values, and then the potential depths (V_0, W_v, and $V_{\rm so}$) are adjusted to improve the fit quality. In the folding model calculations, the renormalization factor (N_r) is fixed as one, and its default value ($\approx$1.0) is not changed. Thus, the effect of N_r on the cross-section calculations is eliminated.

In all the calculations of the $^{14}N(^{17}F, ^{18}Ne)^{13}C$ reaction, $r_w = 1.20$ fm, $a_w = 0.69$ fm, $r_{\rm so} = 0.82$ fm, $a_{\rm so} = 0.35$ fm for $^{17}F + ^{14}N$ channel, $r_v = 1.20$ fm, $a_v = 0.60$ fm, $r_w = 1.20$ fm, $a_w = 0.69$ fm for $^{18}Ne + ^{13}C$ and $^{17}F + ^{13}C$ channels.

In all the calculations of the $^{14}N(^{7}Be, ^{8}B)^{13}C$ reaction, $r_w = 1.20$ fm, $a_w = 0.68$ fm for $^{7}Be + ^{14}N$ channel, $r_v = 1.30$ fm, $a_v = 0.91$ fm, $r_w = 1.36$ fm, $a_w = 1.02$ fm for $^{8}B + ^{13}C$ channel, and $r_v = 0.92$ fm, $a_v = 0.79$ fm, $r_w = 1.03$ fm, $a_w = 0.69$ fm for $^{7}Be + ^{13}C$ channel.

As a result of examining a lot of densities, potentials or NN interactions, it can sometimes be difficult to compare the consistence between the results and the data. In this context, Spatafora *et al.* [56] have introduced a quality factor ($\mathrm{qf}(\theta_i)$) formulated by

$$\mathrm{qf}(\theta_i) = \frac{1}{1 + \left|\ln\frac{\sigma_{\rm theor}(\theta_i)}{\sigma_{\rm exp}(\theta_i)}\right|}, \tag{39}$$

where $\sigma_{\rm exp}$ ($\sigma_{\rm theor}$) is the measured (theoretical) value of the cross-sections at the θ_i scattering angle, respectively. The $\mathrm{qf}(\theta_i)$ can take the values between 0 and 1 corresponding to the worst and best harmonies between the theoretical and the experimental results, respectively. Then the quality factor (QF) values can be obtained for each examined angular distribution as the arithmetic average of the $N_{\rm points}$ measurements at different angles using the formula given by

$$\mathrm{QF} = \frac{\sum_i \mathrm{qf}(\theta_i)}{N_{\rm points}}. \tag{40}$$

In our study, the QF values for all the proton-transfer reactions are calculated and listed in the tables.

7.1. Analysis results of $^{14}N(^{17}F, ^{18}Ne)^{13}C$ reaction

In all the calculations of the $^{14}N(^{17}F, ^{18}Ne)^{13}C$ reaction, the real potential of the entrance channel is obtained by using different density, temperature, potential, and NN interactions together with the spin-orbit potential, while the imaginary part is accepted in the WS form. The real and imaginary potentials of the exit channel and the core-core interaction are assumed as the WS volume potential.

We have first examined the effect of G1, G2, SP, 2pF, Ngo, and S densities of ^{17}F. The radial changes of the DDs are shown comparatively in Fig. 2, *a*. The

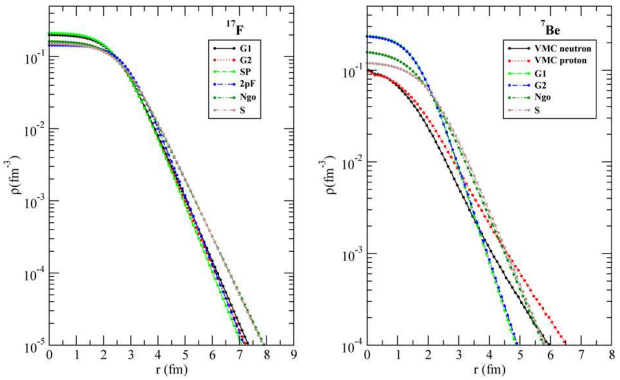

a *b*

Fig. 2. The changes with the distance of (*a*) the G1, G2, SP, 2pF, Ngo and S DDs of ^{17}F, (*b*) the VMC, G1, G2, Ngo and S DDs of ^{7}Be

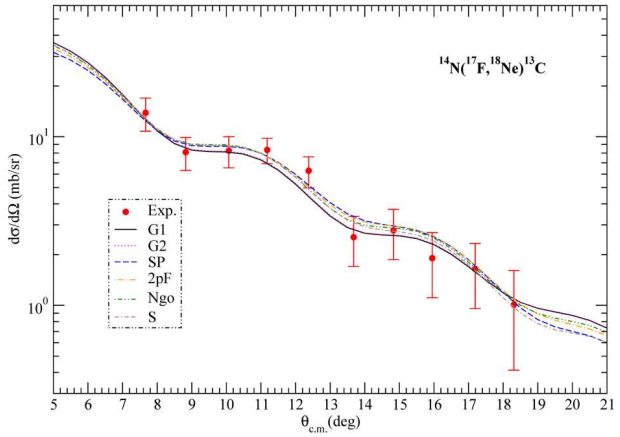

Fig. 3. The cross-sections of ^{14}N(^{17}F, ^{18}Ne)^{13}C for the G1, G2, SP, 2pF, Ngo and S densities at 170 MeV [63]

SP density is the highest in the center, and 2pF is the lowest. However, SP has the shortest tailing, and Ngo has the longest tailing. The cross-sections of ^{14}N(^{17}F, ^{18}Ne)^{13}C proton-transfer reaction at 170 MeV are calculated for the real potentials produced by using these densities within the framework of the DFM, and are demonstrated together with the experimental data in Fig. 3. The OP parameters used in obtaining the theoretical results are supplied in Table 1. The behaviors of SP, 2pF, and Ngo results are close to each other, while the behaviors of G1 and G2 are very similar. It is observed that the agreement of our results with the data is quite better than the literature [57]. It can be said from the QF values that G1, G2 and S are better than the other densities in consistence with the data. However, it is worth mentioning that if several calculations can achieve comparable conformity to the available data or agreement within the experimental error, the inputs of all these calculations (not only the best one) may be regarded as reasonable. Finally, we can express that the G1, G2, and S densities can be especially used as alternative densities for the analysis of the ^{14}N(^{17}F, ^{18}Ne)^{13}C transfer reaction.

It is generally accepted that the initial state of any transfer reaction is at zero temperature [58]. If a nuclear-[interaction collision between the nuclei occurs, an increase in temperature can occur [59, 60]. This effect can cause a change in DDs, and the TD densities can demonstrate differences compared to cold nucleus densities [61]. Moreover, the literature has not enough study to evaluate the TD effect of transfer reactions. Therefore, to apply very unknown TD density in the literature and to propose another approaches in the analysis of transfer reactions can be valuable in explaining both measured data and future transfer studies. For this purpose, we have researched the influence on the ^{14}N(^{17}F, ^{18}Ne)^{13}C transfer cross-section of TD densities of projectile and target in the entrance channel. The 2pF DD is applied for TD cases ($T = 2, 4$, and 6 MeV) and the G1 DD is used for T-IND case ($T = 0$ MeV), while the ^{17}F and ^{14}N densities are calculated. The temperature value is evaluated around 6 MeV as the nucleus can be unstable for much higher temperatures. The radial changes of

Table 1. **The entrance, exit and core-core potential parameters of ^{14}N(^{17}F, ^{18}Ne)^{13}C for different density calculations and quality factors**

Depth	G1	G2	SP	2pF	Ngo	S
^{17}F + ^{14}N						
W_v, MeV	9.10	9.10	12.8	10.30	8.30	13.4
V_{so}, MeV	4.30	4.10	1.00	1.00	1.30	1.00
^{18}Ne + ^{13}C						
V_0, MeV	26.5	26.5	18.0	15.0	15.0	18.0
W_v, MeV	20.0	20.0	21.0	21.0	21.0	15.0
^{17}F + ^{13}C						
V_0, MeV	35.0	35.0	40.0	40.0	40.0	40.0
W_v, MeV	32.6	32.6	22.6	22.6	22.6	22.6
QF	0.90	0.90	0.88	0.88	0.89	0.90

the densities are displayed in Fig. 4, *a* for ^{17}F and in Fig. 4, *b* for ^{14}N. The ^{17}F and ^{14}N densities change with varying the temperature. As a result, the central densities decrease with increasing the temperature, whereas the tailing of densities increase with the temperature. Then we have got the transfer cross-sections for the densities acquired at $T = 0$, 2, 4, and 6 MeV. We have compared our results with the data in Fig. 5, and have listed the OP values for all the channels of the transfer reaction in Table 2. While obtaining the potential parameters, the values providing good harmony results with the data at $T = 0$ MeV are first searched. For $T = 2$, 4, and 6 MeV calculations, we have used, without changing, the potential parameters applied at $T = 0$ MeV. The aim is to evaluate only the TD effect without changing any potential parameter. In this context, we have observed that the results are different from each other according to temperature values. This variation is particularly evident in the results obtained for the TD densities of both ^{17}F and ^{14}N nuclei. As a consequence, we can deduce that the temperature changes the cross-section of the $^{14}N(^{17}F, ^{18}Ne)^{13}C$ reaction.

As far as we know, there is not enough study in the literature to evaluate the proximity type potentials in the transfer analysis. Therefore, it would be meaningful to apply various potentials for the analysis of some proton-transfer reactions. In this manner, we have examined the impress on the cross-section of the $^{14}N(^{17}F, ^{18}Ne)^{13}C$ transfer reaction of nine different proximity-type potentials consisting of Prox 77, Prox 88, AW 95, Bass 73, Bass 77, Bass 80, BW 91, CW 76, and Ngo 80 which their changes according to distance are displayed in Fig. 6. Then the proton-transfer cross-sections, by using these potentials, are calculated for the OP parameters listed in Table 3, and are compared with the data in Fig. 7. The behaviors of the cross-section results based on the proximity potentials have shown similarities and differences for different angles. However, we have realized from the QF values that the Prox 77 and Bass 77 results are slightly better than the other potential results in agreement with the data. In addition, we can see that the theoretical results depend on the choice of the potentials investigated. We can state that the potentials can give different results with each other according to their shapes, and the agreement with the experimental data can increase or decrease [62].

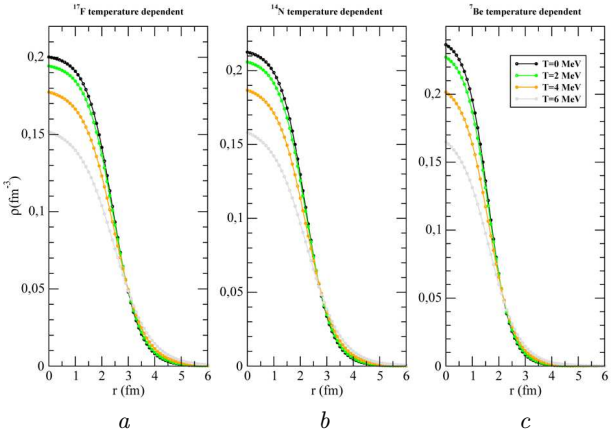

Fig. 4. The changes with the distance of the TD densities for $T = 0, 2, 4$, and 6 MeV of ^{17}F (*a*), ^{14}N (*b*), ^{7}Be (*c*)

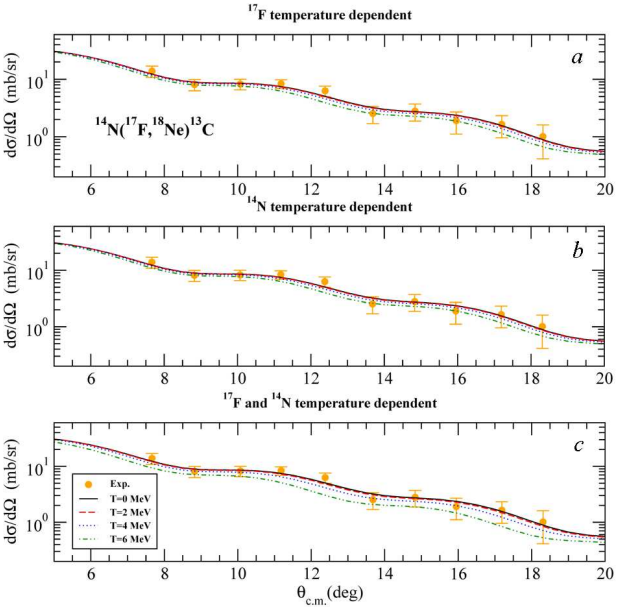

Fig. 5. The cross-sections of $^{14}N(^{17}F, ^{18}Ne)^{13}C$ together with the data [63] for the TD densities of ^{17}F (*a*), ^{14}N (*b*), both ^{17}F and ^{14}N (*c*)

Table 2. **The entrance, exit and core-core potential parameters of $^{14}N(^{17}F, ^{18}Ne)^{13}C$ for TD density calculations**

Channel	V_0, MeV	W_v, MeV	V_{so}, MeV
$^{17}F + ^{14}N$	–	20.0	1.0
$^{18}Ne + ^{13}C$	18.0	15.0	–
$^{17}F + ^{13}C$	40.0	22.6	–

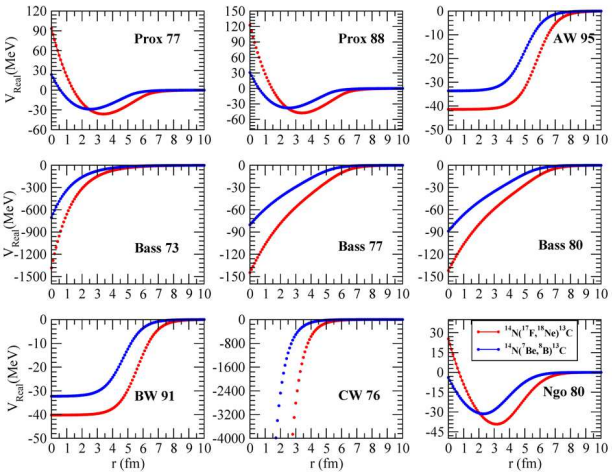

Fig. 6. Distance-dependent changes of Prox 77, Prox 88, AW 95, Bass 73, Bass 77, Bass 80, BW 91, CW 76, and Ngo 80 for ^{14}N(^{17}F, ^{18}Ne)^{13}C and ^{14}N(^{7}Be, ^{8}B)^{13}C

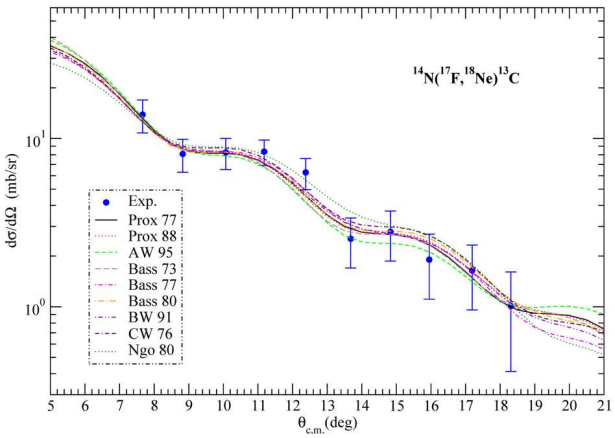

Fig. 7. The cross-sections of ^{14}N(^{17}F, ^{18}Ne)^{13}C for Prox 77, Prox 88, AW 95, Bass 73, Bass 77, Bass 80, BW 91, CW 76, and Ngo 80 together with the data [63]

Finally, we have examined the impact of NN interactions on the transfer cross-section of HS, Z, W, L1, L2, L3, TS, NL1, NL2, NL3 and NL3*. The real potentials of the entrance channel are produced by using these NN interactions and the G1 density for the ^{17}F and ^{14}N nuclei, and the radial changes of all the NN interactions are shown in Fig. 8, *a*. It is experienced that the shallowest potential is for NL2, and the deepest potential is for L2. Then, the transfer results together with the data are displayed in Fig. 9, and the OP parameters are given in Table 4. The results with different NN interaction show similarities and differences. The QF values indicate that the Z,

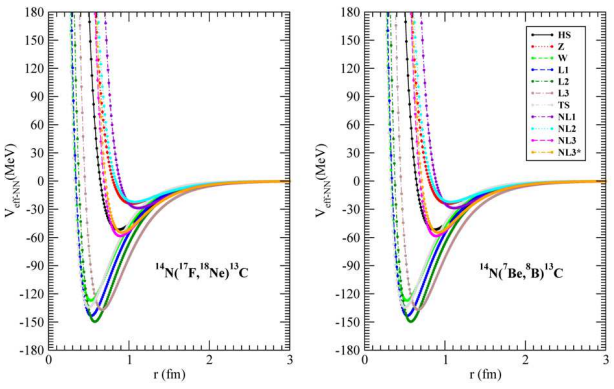

Fig. 8. Distance-dependent changes of the HS, Z, W, L1, L2, L3, TS, NL1, NL2, NL3 and NL3* interactions for (*a*) ^{14}N(^{17}F, ^{18}Ne)^{13}C, (*b*) ^{14}N(^{7}Be, ^{8}B)^{13}C

NL1, NL2, NL3, and NL3* results are generally far from describing the experimental data. Moreover, we have realized that the HS, L2, and TS results are better than the other NN results in agreement with the data.

7.2. Analysis results of ^{14}N(^{7}Be, ^{8}B)^{13}C reaction

For all the theoretical calculations of the ^{14}N(^{17}F, ^{18}Ne)^{13}C reaction, the real part of the entrance channel is produced by using different densities, temperatures, potentials, and NN interactions, while the

Table 3. **The entrance, exit and core-core potential parameters of ^{14}N(^{17}F, ^{18}Ne)^{13}C for different nuclear potential calculations and quality factors**

Depth	Prox 77	Prox 88	AW 95	Bass 73	Bass 77	Bass 80	BW 91	CW 76	Ngo 80
^{17}F + ^{14}N									
W_v, MeV	8.60	10.6	6.60	4.60	12.6	9.30	12.3	10.3	17.3
V_{so}, MeV	1.00	1.70	4.10	1.70	1.00	1.00	2.00	2.00	2.00
^{18}Ne + ^{13}C									
V_0, MeV	38.2	32.0	25.0	15.0	25.0	25.0	20.0	20.0	20.0
W_v, MeV	19.1	19.1	23.0	22.0	22.0	22.0	21.0	17.0	21.0
^{17}F + ^{13}C									
V_0, MeV	40.2	40.0	40.0	40.0	40.0	40.0	40.0	40.0	40.0
W_v, MeV	23.6	23.6	23.6	22.6	22.6	22.6	22.6	42.6	22.6
QF	0.91	0.90	0.89	0.90	0.91	0.89	0.90	0.88	0.87

imaginary part is taken as WS. Both real and imaginary parts of the exit channel and the core-core interaction are assumed as the WS volume potential.

In the first stage, the effects of VMC, G1, G2, Ngo, and S densities of the ^{7}Be projectile whose radial changes are presented in Fig. 2, *b* on the entrance channel are investigated. The G1 density has the shortest tailing, and the VMC proton density has the longest tailing. Then the reaction cross-sections of ^{14}N(^{7}Be, ^{8}B)^{13}C at 84 MeV' where the real potentials are achieved for the analyzed densities' by using the DFM, are shown together with the data in Fig. 10,

Table 4. **The entrance, exit and core-core potential parameters of ^{14}N(^{17}F, ^{18}Ne)^{13}C for different *NN* interaction calculations and quality factors**

Depth	HS	Z	W	L1	L2	L3	TS	NL1	NL2	NL3	NL3*
^{17}F + ^{14}N											
W_v, MeV	9.60	30.0	6.60	4.60	5.60	5.60	7.00	27.0	37.0	39.0	39.0
V_{so}, MeV	1.10	4.10	3.10	3.10	1.10	1.10	1.10	1.10	1.10	1.10	1.10
^{18}Ne + ^{13}C											
V_0, MeV	22.0	32.0	22.0	12.0	12.0	10.0	22.0	40.0	40.0	42.0	42.0
W_v, MeV	25.0	16.0	25.0	25.0	13.0	11.0	25.0	11.0	11.0	7.00	7.00
^{17}F + ^{13}C											
V_0, MeV	40.0	20.0	40.0	40.0	40.0	60.0	50.0	20.0	30.0	20.0	20.0
W_v, MeV	23.6	23.6	23.6	23.6	21.6	18.6	23.6	18.6	18.6	33.6	50.0
QF	0.89	0.84	0.88	0.87	0.89	0.88	0.89	0.73	0.83	0.83	0.83

Table 5. **The entrance, exit and core-core potential parameters of ^{14}N(^{7}Be, ^{8}B)^{13}C for different density calculations and quality factors**

Depth	VMC	G1	G2	Ngo	S
^{7}Be + ^{14}N					
W_v, MeV	7.60	10.0	10.0	8.30	8.30
^{8}B + ^{13}C					
V_0, MeV	51.2	51.2	51.2	51.2	51.2
W_v, MeV	28.3	28.3	28.3	28.3	28.3
^{7}Be + ^{13}C					
V_0, MeV	47.0	47.0	47.0	47.0	47.0
W_v, MeV	41.9	41.9	41.9	41.9	41.9
QF	0.76	0.78	0.78	0.77	0.77

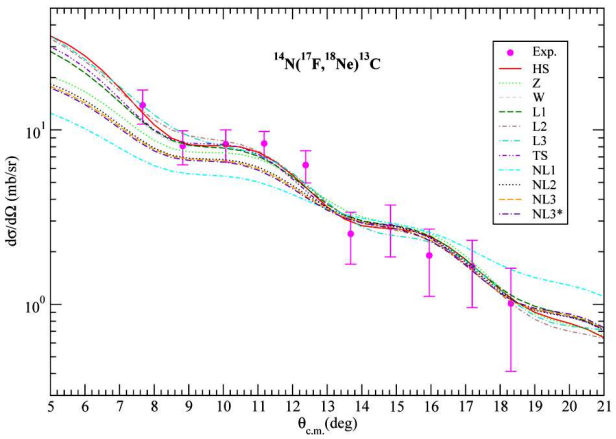

Fig. 9. The cross-sections of ^{14}N(^{17}F, ^{18}Ne)^{13}C for the HS, Z, W, L1, L2, L3, TS, NL1, NL2, NL3 and NL3* interactions together with the data [63]

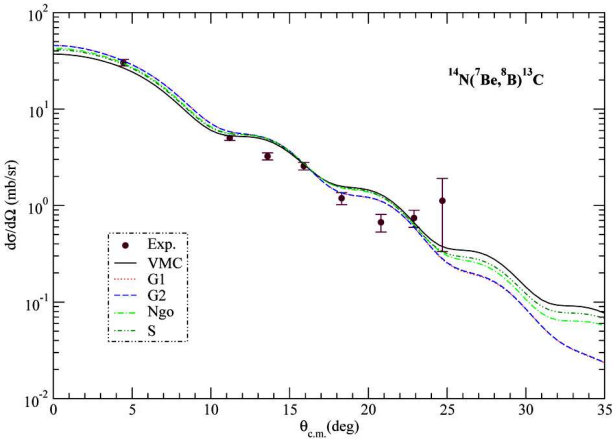

Fig. 10. The cross-sections of ^{14}N(^{7}Be, ^{8}B)^{13}C for the VMC, G1, G2, Ngo, and S densities at 84 MeV [63]

and the OP parameters are listed in Table 5. The Ngo and S results are very similar to each other, while the G1 and G2 results are almost the same. Moreover, the results with the G1 and G2 densities are slightly better than the other density results in agreement with the data based on the QF values. Thus, we can conclude that the G1 and G2 densities can be especially used as alternative DDs for the analysis of the ^{14}N(^{7}Be, ^{8}B)^{13}C transfer reaction.

We have researched the influence on the reaction cross-section of TD densities of both projectile and target in the entrance channel. The TD (T = 2, 4 and 6 MeV) and T-IND (T = 0 MeV) densities are calculated, and the radial changes of the densities

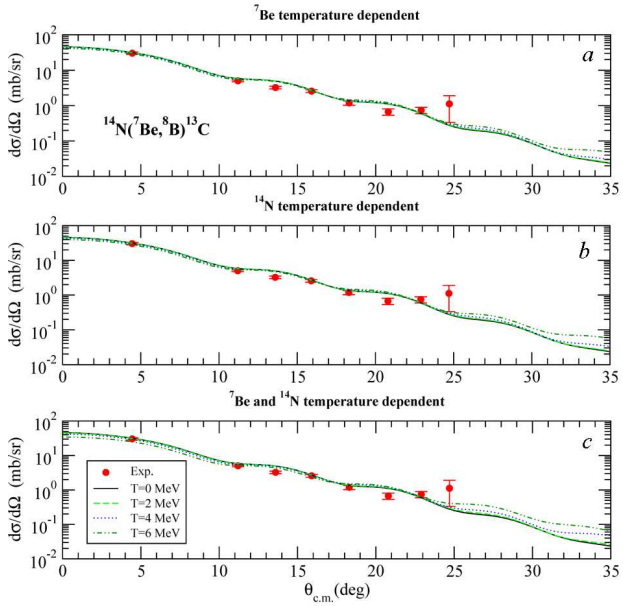

Fig. 11. The cross-sections of ^{14}N(^{7}Be, ^{8}B)^{13}C together with the data [63] for the TD densities of ^{7}Be (*a*), ^{14}N (*b*), both ^{7}Be and ^{14}N nuclei (*c*)

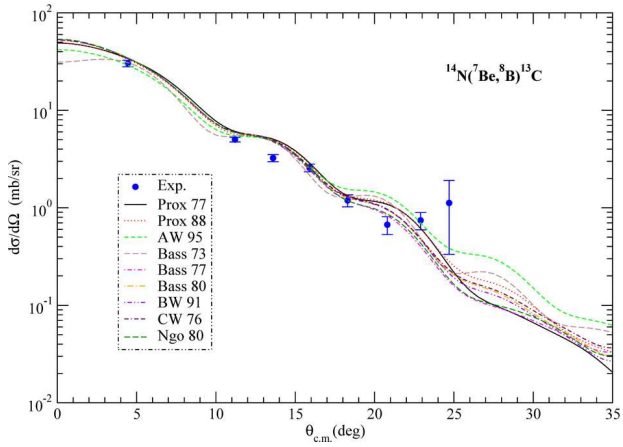

Fig. 12. The cross-sections of ^{14}N(^{7}Be, ^{8}B)^{13}C for Prox 77, Prox 88, AW 95, Bass 73, Bass 77, Bass 80, BW 91, CW 76, and Ngo 80 together with the data [63]

are presented in Fig. 4, *b* for ^{14}N and in Fig. 4, *c* for ^{7}Be. The G1 DD is used for T-IND case of the ^{7}Be and ^{14}N nuclei. In this context, the densities in the center decrease with increasing the temperature, r.e., whereas the tailing of densities increase with increasing the temperature. Then we have obtained the transfer cross-section results for the densities produced at $T = 0$, 2, 4, and 6 MeV, and have compared the theoretical results and the data in Fig. 11. The potential sets for each channel are also presented in table 6. While finding the OP parameters, the method applied in the analysis of the ^{14}N(^{17}F, ^{18}Ne)^{13}C reaction is followed. The results from $T = 2$ MeV to $T = 6$ MeV are different from each other, but this difference is not high. As a consequence, it can be deduced that the temperature changes the cross-section somewhat. It is evident from the results that the effect of the temperature on the DD changes much less the cross-sections of the ^{14}N(^{7}Be, ^{8}B)^{13}C reaction compared to the ^{14}N(^{17}F, ^{18}Ne)^{13}C reaction. As a reason for this, we think that the differences in the TD analysis may be due to the differences in the number of nucleons of the nuclei. In other words, the presence of more nucleons in the nucleus would generate a greater temperature effect on the DD, and, thusly there would be differences between the results.

The determination of potential parameters for the analysis of transfer reactions is difficult. If the number of free parameters of the applied potentials in the theoretical calculations increases, the analysis becomes more difficult. In other words, it is very significant to determine a suitable potential that explains the nuclear reaction. Thus, revealing the alternative nuclear potentials is very useful to determine transfer reactions. For this purpose, the impression on the proton-transfer cross-section of the Prox 77, Prox 88, AW 95, Bass 73, Bass 77, Bass 80, BW 91, CW 76, and Ngo 80 is examined, and variation with distance of the potentials is shown in Fig. 6. From this point of view, the transfer cross-sections are calculated by using the OP parameters given in Table 7, and the results with the data are compared in Fig. 12. The behaviors of the results based on the proximity potentials show similarities and differences. In addition to this, it is found that the potential results have

Table 6. **The entrance, exit, and core-core potential parameters of ^{14}N(^{7}Be, ^{8}B)^{13}C for TD density calculations**

Channel	V_0, MeV	W_v, MeV
^{7}Be + ^{14}N	–	10.0
^{8}B + ^{13}C	51.2	28.3
^{7}Be + ^{13}C	47.0	41.9

approximately similar success over the average in describing the experimental data.

Lastly, the effect of HS, Z, W, L1, L2, L3, TS, NL1, NL2, NL3, and NL3* NN interactions on the transfer cross-section is determined. For this, the real potential of the entrance channel of $^{14}N(^{7}Be, ^{8}B)^{13}C$ is calculated by using these NN interactions whose radial changes are showed in Fig. 8, *b*. The shallowest potential is for NL2, and the deepest potential is for L2. Then the calculated transfer cross-sections are displayed in Fig. 13, and the OP parameters of all the

Table 7. **The entrance, exit and core-core potential parameters of $^{14}N(^{7}Be, ^{8}B)^{13}C$ for different nuclear potential calculations and quality factors**

Depth	Prox 77	Prox 88	AW 95	Bass 73	Bass 77	Bass 80	BW 91	CW 76	Ngo 80
$^{7}Be + ^{14}N$									
W_v, MeV	9.00	9.00	10.0	10.0	27.0	20.0	21.0	19.0	26.0
$^{8}B + ^{13}C$									
V_0, MeV	55.2	51.2	51.2	11.2	47.2	55.2	55.2	55.2	55.2
W_v, MeV	27.3	28.3	28.3	22.3	24.3	22.3	22.3	22.3	22.3
$^{7}Be + ^{13}C$									
V_0, MeV	50.0	47.0	47.0	27.0	57.0	37.0	27.0	27.0	27.0
W_v, MeV	36.9	41.9	41.9	31.9	51.9	31.9	31.9	31.9	31.9
QF	0.78	0.78	0.77	0.78	0.78	0.77	0.77	0.77	0.78

Table 8. **The entrance, exit and core-core potential parameters of $^{14}N(^{7}Be, ^{8}B)^{13}C$ for different NN interaction calculations and quality factors**

Depth	HS	Z	W	L1	L2	L3	TS	NL1	NL2	NL3	NL3*
$^{7}Be + ^{14}N$											
W_v, MeV	8.00	36.0	36.0	8.00	8.00	8.00	34.0	48.0	37.0	37.0	36.0
$^{8}B + ^{13}C$											
V_0, MeV	70.2	54.5	45.0	57.2	53.0	41.0	48.0	51.0	51.0	53.0	53.0
W_v, MeV	28.3	21.0	21.0	28.3	28.3	28.3	21.0	22.0	21.5	21.0	21.0
$^{7}Be + ^{13}C$											
V_0, MeV	53.0	48.0	48.0	53.0	53.0	54.0	48.0	54.0	50.0	48.0	48.0
W_v, MeV	41.9	39.9	39.9	41.9	41.9	39.9	39.9	39.9	39.9	39.9	39.9
QF	0.80	0.78	0.78	0.77	0.77	0.77	0.77	0.73	0.77	0.77	0.77

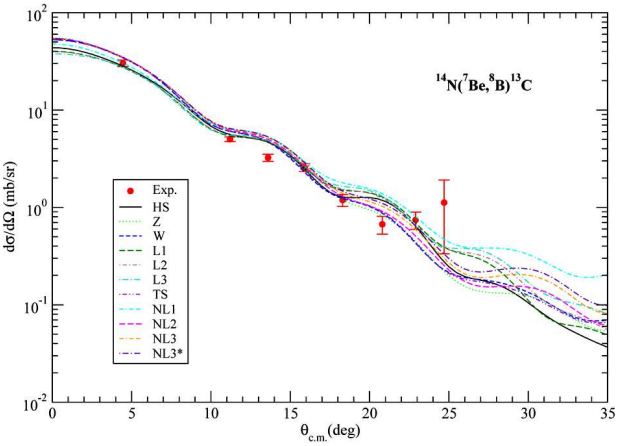

Fig. 13. The cross-sections of $^{14}N(^{7}Be, ^{8}B)^{13}C$ for the HS, Z, W, L1, L2, L3, TS, NL1, NL2, NL3, and NL3* interactions together with the data [63]

NN interactions are provided in Table 8. The behaviors of the results with the Z-W, and L1-L2-L3, and NL3-NL3* interactions are similar among themselves, and the NL1 result is generally far from describing the data. The NN interaction results except for HS have approximately similar success over the average in describing the data. Additionally, it can be said from the QF values that the result with the HS interaction is better than the other NN interaction results in agreement with the data.

8. Summary and Conclusions

In the present study, we have focused on a comprehensive review of the $^{14}N(^{17}F, ^{18}Ne)^{13}C$ at 170 MeV and $^{14}N(^{7}Be, ^{8}B)^{13}C$ at 84 MeV proton-transfer reactions by using different DDs, temperature cases, nuclear potentials, and NN interactions. We have calculated the reaction cross-sections within the code FRESCO based on the DWBA method.

We have proposed alternative DDs which can be used in the theoretical analysis of each transfer reaction. In this respect, the G1, G2, and S densities for $^{14}N(^{17}F, ^{18}Ne)^{13}C$ and the G1 and G2 densities for $^{14}N(^{7}Be, ^{8}B)^{13}C$ can be especially applied as alternative densities. It should also be noted that G1 and G2 are common densities for both reactions. Therefore, it can be stated that G1 and G2 densities would be very useful for the analysis of the transfer reactions examined in this study.

Then we have observed that the TD density has changed the transfer cross-section in both reactions. In addition, it has been realized that the TD density changes more the ^{14}N(^{17}F, ^{18}Ne)^{13}C cross-section compared to the ^{14}N(^{7}Be, ^{8}B)^{13}C reaction. We think that the reason for this may be the differences in the number of nucleons in the ^{17}F and ^{7}Be nuclei.

We have also examined different nuclear potentials in analyzing the transfer reactions, and have provided alternative potentials. Moreover, it has been seen that the Prox 77 and Bass 77 results are slightly better than the other potential results in agreement with the data for the ^{14}N(^{17}F, ^{18}Ne)^{13}C reaction while the potential results analyzed for ^{14}N(^{17}F, ^{18}Ne)^{13}C have approximately similar success over the average in describing the experimental data.

Finally, we have researched the effect of various NN interactions in explaining the transfer cross-section, and have presented alternative NN interactions to the M3Y interaction for the theoretical analysis of each proton-transfer reaction analyzed with this study. In this manner, it can be said that the HS, L2, and TS interactions for ^{14}N(^{17}F, ^{18}Ne)^{13}C and the HS interaction for the ^{14}N(^{7}Be, ^{8}B)^{13}C reaction can be especially evaluated as alternative NN interactions. Additionally, it can be seen that the HS interaction is common interaction for both reactions. Thus, the conclusion can be drawn that the HS interaction would be beneficial for the analysis of the proton-transfer reactions examined in this study.

Consequently, we believe that it would be interesting and useful to experience these approaches to another transfer reactions.

The authors are very grateful to the Scientific and Technological Research Council of Türkiye (TUBITAK) for the financial support (Project No. 122F275).

1. H.A. Bethe. Energy production in stars. *Phys. Rev.* **55**, 103 (1939).
2. E.M. Burbidge, G.R. Burbidge, W.A. Fowler, F. Hoyle. Synthesis of the elements in stars. *Rev. Mod. Phys.* **29**, 547 (1957).
3. M.S. Smith, D.W. Bardayan, J.C. Blackmon, E. Browne, R.B. Firestone, G.M. Hale, R.D. Hoffman, Z. Ma, V. McLane, E.B. Norman, N. Shu, D.L. Smith, L.A. Van Wormer, S.E. Woosley, S. Wu. Recent nuclear astrophysics data activities in the U.S. *AIP Conference Proceedings* **529**, 243 (2000).
4. P. Descouvemont. Nuclear reactions of astrophysical interest. *Front. Astron. Space Sci.* **7**, 9 (2020).
5. H.M. Xu, C.A. Gagliardi, R.E. Tribble, A.M. Mukhamedzhanov, N.K. Timofeyuk. Overall normalization of the astrophysical factor and the nuclear vertex constant for reactions. *Phys. Rev. Lett.* **73**, 2027 (1994).
6. C.A. Gagliardi, R.E. Tribble, J. Jiang, A.M. Mukhamedzhanov, L. Trache, H.M. Xu, S.J. Yennello, X.G. Zhou. Determining S^{17}(0) from the ^{10}B(^{7}Be, ^{8}B)^{9}Be reaction. *Nucl. Phys. A* **588**, c327 (1995).
7. J.G. Ross, J. Görres, C. Iliadis, S. Vouzoukas, M. Wiescher, R.B. Vogelaar, S. Utku, N.P.T. Bateman, P.D. Parker. Indirect study of low-energy resonances in ^{31}P(p,α)^{28}Si and ^{35}Cl(p,α)^{32}S. *Phys. Rev. C* **52**, 1681 (1995).
8. L. Trache, A. Azhari, H.L. Clark, C.A. Gagliardi, Y.-W. Lui, A.M. Mukhamedzhanov, R.E. Tribble, F. Carstoiu. Optical model potentials involving loosely bound p-shell nuclei around 10 MeV/nucleon. *Phys. Rev. C* **61**, 024612 (2000).
9. I.J. Thompson. *Getting Started with FRESCO*, unpublished (2010).
10. R. Chatterjee, J. Okołowicz, M. Płoszajczak. Description of the ^{17}F(p, γ)^{18}Ne radiative capture reaction in the continuum shell model. *Nucl. Phys. A* **764**, 528 (2006).
11. S.D. Pain. Advances in instrumentation for nuclear astrophysics. *AIP Advances* **4**, 041015 (2014).
12. J.C. Blackmon (for the RIBENS Collaboration). Spectroscopy with radioactive ion beams at the HRIBF for nuclear astrophysics. *J. Phys. G: Nucl. Part. Phys.* **31**, S1405 (2005).
13. M. Wiescher, J. Görres, F.K. Thielemann. ^{17}F(p,γ)^{18}Ne in explosive hydrogen burning. *Astrophys. J.* **326**, 384 (1988).
14. S.S. Chandel, S.K. Dhiman, R. Shyam. Structure of ^{8}B and astrophysical S_{17} factor in Skyrme Hartree-Fock theory. *Phys. Rev. C* **68**, 054320 (2003).
15. A. Azhari, V. Burjan, F. Carstoiu, C.A. Gagliardi, V. Kroha, A.M. Mukhamedzhanov, X. Tang, L. Trache, R.E. Tribble. The ^{14}N(^{7}Be,^{8}B)^{13}C reaction and the ^{7}Be(p,γ)^{8}B S factor. *Phys. Rev. C* **60**, 055803 (1999).
16. A.M. Moro, R. Crespo, F.M. Nunes, I.J. Thompson. Breakup and core coupling in ^{14}N(^{7}Be,^{8}B)^{13}C. *Phys. Rev. C* **67**, 047602 (2003).
17. A.M. Moro, R. Crespo, F.M. Nunes, I.J. Thompson. ^{8}B breakup in elastic and transfer reactions. *Phys. Rev. C* **66**, 024612 (2002).
18. I.J. Thompson. Coupled reaction channels calculations in nuclear physics. *Comp. Phys. Rep.* **7**, 167 (1988).
19. J. Cook. DFPOT – A program for the calculation of double folded potentials. *Commun. Comput. Phys.* **25**, 125 (1982).
20. M. Aygun. Comprehensive research of ^{10}C nucleus using different theoretical approaches. *Ukr. J. Phys.* **66**, 8 (2021).
21. M. Aygun. A comparison of proximity potentials in the analysis of heavy-ion elastic cross sections. *Ukr. J. Phys.* **63**, 881 (2018).

22. M. Aygun. Effects of proximity potentials on the cross-sections of ^{6,8}He + ^{65}Cu halo fusion reactions. *Ukr. J. Phys.* **64**, 363 (2019).
23. M. Aygun. A comparative analysis of the density distributions and the structure models of ^{9}Li. *Pramana – J. Phys.* **88**, 53 (2017).
24. M. Aygun, Z. Aygun, N. Karaali. A comprehensive analysis of ^{26}Mg(^{3}H,^{2}H)^{27}Mg reaction at 36 MeV. *Rev. Mex. Fìs.* **69**, 051201 (2023).
25. M. Aygun, Z. Aygun, N. Karaali. Analysis of ^{6}Li(^{3}He, d)^{7}Be transfer reaction for different approaches. *Acta Phys. Pol. B* **54**, 5-A1 (2023).
26. A.A. Ibraheem, M. Aygun, N.A.M. Alsaif, A. Alghamdi, Sh. Hamada. Analysis of d + ^{6,7,9,11}Li elastic scattering using different densities and calculation procedures. *Phys. Scr.* **97**, 085304 (2022).
27. R.K. Gupta, D. Singh, W. Greiner. Semiclassical and microscopic calculations of the spin-orbit density part of the Skyrme nucleus-nucleus interaction potential with temperature effects included. *Phys. Rev. C* **75**, 024603 (2007).
28. O.N. Ghodsi, F. Torabi. Comparative study of fusion barriers using Skyrme interactions and the energy density functional. *Phys. Rev. C* **92**, 064612 (2015).
29. R.K. Gupta, D. Singh, R. Kumar, W. Greiner. Universal functions of nuclear proximity potential for Skyrme nucleusпїЅnucleus interaction in a semiclassical approach. *J. Phys. G: Nucl. Part. Phys.* **36**, 075104 (2009).
30. L.C. Chamon, B.V. Carlson, L.R. Gasques, D. Pereira, C. De Conti, M.A.G. Alvarez, M.S. Hussein, M.A. CrїSndido Ribeiro, E.S. Rossi, Jr., C.P. Silva. Toward a global description of the nucleus-nucleus interaction. *Phys. Rev. C* **66**, 014610 (2002).
31. W.M. Seif, H. Mansour. Systematics of nucleon density distributions and neutron skin of nuclei. *Int. J. Mod. Phys. E* **24**, 1550083 (2015).
32. C. Ngô, B. Tamain, M. Beiner, R.J. Lombard, D. Mas, H.H. Deubler. Properties of heavy ion interaction potentials calculated in the energy density formalism. *Nucl. Phys. A* **252**, 237 (1975).
33. H. Ngô, C. Ngô. Calculation of the real part of the interaction potential between two heavy ions in the sudden approximation. *Nucl. Phys. A* **348**, 140 (1980).
34. H. Schechter, L.F. Canto. Proximity formulae for folding potentials. *Nucl. Phys. A* **315**, 470 (1979).
35. S.C. Pieper, K. Varga, R.B. Wiringa. Quantum Monte Carlo calculations of $A = 9$, 10 nuclei. *Phys. Rev. C* **66**, 044310 (2002).
36. https://www.phy.anl.gov/theory/research/density/.
37. D. Singh, R.K. Gupta. *Proceedings of DAE-BRNS Symposium on Nuclear Physics, Mumbai, India* (2003), Vol. B46, p. 254.
38. S. Shlomo, J.B. Natowitzi. Temperature and mass dependence of level density parameter. *Phys. Rev. C* **44**, 2878 (1991).
39. J. Blocki, J. Randrup, W.J. Swiatecki, C.F. Tsang. Proximity forces. *Ann. Phys. (NY)* **105**, 427 (1977).
40. I. Dutt, R.K. Puri. Comparison of different proximity potentials for asymmetric colliding nuclei. *Phys. Rev. C* **81**, 064609 (2010).
41. W.D. Myers, W.J. Swiatecki. Nuclear masses and deformations. *Nucl. Phys.* **81**, 1 (1966).
42. W. Reisdorf. Heavy-ion reactions close to the Coulomb barrier. *J. Phys. G: Nucl. Part. Phys.* **20**, 1297 (1994).
43. L. Zhang, Y. Gao, H. Zheng, M.R. Huang, X. Liu. Moments of the three-parameter Fermi distribution. *Mod. Phys. Lett. A* **32**, 1750195 (2017).
44. A. Winther. Dissipation, polarization and fluctuation in grazing heavy-ion collisions and the boundary to the chaotic regime. *Nucl. Phys. A* **594**, 203 (1995).
45. R. Bass. Threshold and angular momentum limit in the complete fusion of heavy ions. *Phys. Lett. B* **47**, 139 (1973).
46. R. Bass. Fusion of heavy nuclei in a classical model. *Nucl. Phys. A* **231**, 45 (1974).
47. R. Bass. Nucleus-nucleus potential deduced from experimental fusion cross sections. *Phys. Rev. Lett.* **39**, 265 (1977).
48. P.R. Christensen, A. Winther. The evidence of the ion-ion potentials from heavy ion elastic scattering. *Phys. Lett. B* **65**, 19 (1976).
49. P.G. Reinhard. The relativistic mean-field description of nuclei and nuclear dynamics. *Rep. Prog. Phys.* **52**, 439 (1989).
50. H. Toki, Y. Sugahara, D. Hirata, B.V. Carlson, I. Tanihata. Properties of nuclei far from the stability line in the relativistic hartree theory. *Nucl. Phys. A* **524**, 633 (1991).
51. G.A. Lalazissis, J. König, P Ring. New parametrization for the Lagrangian density of relativistic mean field theory. *Phys. Rev. C* **55**, 540 (1997).
52. G. Lalazissis, S. Karatzikos, R. Fossion, D. Pena Arteaga, A.V. Afanasjev, P. Ring. The effective force NL3 revisited. *Phys. Lett. B* **671**, 36 (2009).
53. L.D. Miller, A.E.S. Green. Relativistic self-consistent meson field theory of spherical nuclei. *Phys. Rev. C* **5**, 241 (1972).
54. R. Brockmann, W. Weise. Spin-orbit coupling in a relativistic Hartree model for finite nuclei. *Phys. Rev. C* **16**, 1282 (1977).
55. R. Brockmann. Relativistic Hartree–Fock description of nuclei. *Phys. Rev. C* **18**, 1510 (1978).
56. A. Spatafora *et al.* (NUMEN Collaboration). Multichannel experimental and theoretical approach to the ^{12}C(^{18}O,^{18} F)^{12}B single-charge-exchange reaction at 275 MeV: Initial-state interaction and single-particle properties of nuclear wave functions. *Phys. Rev. C* **107**, 024605 (2023).
57. J.C. Blackmon *et al.* The ^{17}F(p, γ)^{18}Ne direct capture cross section. *Nucl. Phys. A* **746**, 365c (2004).
58. M. Aygun, Z. Aygun. A comprehensive analysis of ^{9}Li + + ^{70}Zn fusion cross section by using proximity potentials,

temperature dependent density distributions and nuclear potentials. *Rev. Mex. Fis.* **65**, 573 (2019).
59. L. Guo-Qiang, X. Gong-Ou. Optical potential and the fusion barrier of two hot nuclei. *Phys. Rev. C* **41**, 169 (1990).
60. M. Rashdan, A. Faessler, M. Ismail, N. Ohtsuka. The temperature dependence of the Hi optical potential. *Nucl. Phys. A* **468**, 168 (1987).
61. R.K. Puri, N. Ohtsuka, E. Lehmann, A. Faessler, M.A. Matin, Dao T. Khoa, G. Batko, S.W. Huang. Temperature-dependent mean field and its effect on heavy-ion reactions. *Nucl. Phys. A* **575**, 733 (1994)
62. M. Aygun. Comparative analysis of proximity potentials to describe scattering of ^{13}C projectile off ^{12}C, ^{16}O, ^{28}Si and ^{208}Pb nuclei. *Rev. Mex. Fis.* **64**, 149 (2018).
63. https://www-nds.iaea.org/exfor/.

Received 28.11.23

М. Айгун, З. Айгун, Н. Караалі

ПОВНИЙ АНАЛІЗ РЕАКЦІЙ ^{14}N(^{17}F, ^{18}Ne)^{13}C ТА ^{14}N(^{7}Be, ^{8}B)^{13}C З ПЕРЕДАЧЕЮ ПРОТОНА, ЯКІ ЗАЛЕЖАТЬ ВІД ТЕМПЕРАТУРИ, РОЗПОДІЛУ ГУСТИНИ, ЯДЕРНОГО ПОТЕНЦІАЛУ І ВЗАЄМОДІЇ МІЖ НУКЛОНАМИ

Досліджено кутові розподіли реакцій ^{14}N(^{17}F, ^{18}Ne)^{13}C при 170 МеВ та ^{14}N(^{7}Be, ^{8}B)^{13}C при 84 МеВ з передачею протона, які залежать від розподілів густини, температури, ядерних потенціалів і взаємодії нуклонів. Розрахунки виконано кодом FRESCO у наближенні деформованих хвиль Борна. Отримані результати порівнюються з іншими теоретичними роботами і з експериментальними даними.

Ключові слова: реакція з передачею частинки, розподіл густини, ядерний потенціал, нуклон-нуклонна взаємодія.